



# Phase transformation/stabilization and ionic conductivity in tantalum oxide co-doped zirconia-scandia solid electrolyte

J. P. Souza<sup>1</sup> · T. G. Fujimoto<sup>1,2</sup> · R. M. Batista<sup>1</sup> · M. C. Steil<sup>2</sup> · R. Muccillo<sup>1</sup> · E. N. S. Muccillo<sup>1</sup>

Received: 1 April 2022 / Revised: 4 May 2022 / Accepted: 6 May 2022 / Published online: 13 May 2022  
© The Author(s), under exclusive licence to Springer-Verlag GmbH Germany, part of Springer Nature 2022

## Abstract

The influence of small amounts of tantalum oxide as co-dopant on phase transformation and stabilization, microstructure and ionic conductivity of zirconia-10 mol% scandia is reported in this work. Cylindrical pellets were prepared by solid state synthesis with sintering at 1500 °C for 5 h. High relative density values (> 95%) were achieved. Reduction of the enthalpy for the cubic  $\rightleftharpoons\beta$ -rhombohedral phase transformation was found for increasing amounts of the co-dopant. Full stabilization of the cubic structure at room temperature was obtained with only 0.45 mol% tantalum oxide addition. The ionic conductivity of sintered specimens was investigated as a function of the temperature and oxygen partial pressure by impedance spectroscopy. The fully stabilized co-doped system revealed a pure ionic conduction behavior up to 800 °C with wide electrolytic domain. In the 700–800 °C range, the ionic conductivity of co-doped specimens is similar to that of pure zirconia-scandia.

**Keywords** Zirconia ceramics · Phase transformation · Microstructure · Transport properties · Solid electrolyte

## Introduction

Many functional ceramics achieve their special properties by doping. Zirconia-based ceramics are good examples, where dopants play a key role for determining their outstanding electrical and mechanical properties, leading to a wide range of technological applications [1, 2]. The high ionic conductivity of doped zirconias, for instance, is assigned to a substantial increase in the concentration of charge carriers (oxygen vacancies), with the introduction of specific amounts of acceptor dopants [2, 3]. The highest values of the ionic conductivity in zirconia systems are usually found for cubic stabilized ceramics, and close to the boundary between the tetragonal and cubic phase fields [2, 3]. Then, for those applications of doped zirconias foreseeing high ionic conductivity, full stabilization at room temperature of the high symmetry cubic phase is required.

Among the zirconia systems, that containing scandium exhibits an intriguing behavior. The phase diagram reveals

seven crystallographic phases: monoclinic (m), tetragonal (t), non-transformable tetragonal (t'), cubic (c), and three polymorphs with rhombohedral symmetry ( $\beta$ ,  $\gamma$ , and  $\delta$ ) [4]. Moreover, a tetragonal (t'') is found in nanostructured zirconia-scandia [5]. Pure cubic phase in this system is barely obtained at room temperature at any scandium content under thermodynamic equilibrium. This effect may be understood taking into account the enthalpies of phase formation [6]. The ionic conductivity value is maximized in the 9–10 mol% scandium range. Nonetheless, thermal degradation of the ionic conductivity occurs at a non-negligible rate above 850 °C mainly in the presence of t' phase; and close to 10 mol% content, the cubic phase spontaneously transforms to the  $\beta$ -rhombohedral phase during cooling down from the sintering temperature [7].

The cubic  $\rightleftharpoons\beta$ -rhombohedral phase transformation in zirconia-scandia was studied by a number of techniques [7–9]. It was shown that this is a first-order and reversible phase transformation exhibiting thermal hysteresis in the 500 to 600 °C range. The  $\beta$ -rhombohedral phase shows vacancy ordering [9], thereby decreasing the concentration of oxygen vacancies available for conduction, and consequently, it is a low conducting phase.

The main strategy to overcome these undesirable effects in zirconia-scandia and to stabilize at room temperature, the high ionic conductivity cubic phase has been the

✉ E. N. S. Muccillo  
enavarro@usp.br

<sup>1</sup> Center of Materials Science and Technology - IPEN, PO Box 11049, São Paulo, SP, Brazil

<sup>2</sup> CNRS, Grenoble INP, LEPMI, University of Grenoble-Alpes, Gieres, France

introduction of a co-dopant. All investigated co-dopants have demonstrated to be efficient for stabilizing the cubic phase to some extent and to increase the ionic conductivity in the low temperature range (up to  $\sim 550$  °C) [10–19]. Despite these regular features, the minimum co-dopant concentration for full stabilization of the cubic phase, the relative increase of the ionic conductivity at low temperatures, the degradation of the conductivity with subsequent thermal annealing, and the ionic conductivity at intermediate temperatures (from  $\sim 550$  to  $\sim 800$  °C), seem to be characteristics of each specific co-dopant.

It is generally known that in polycrystalline materials, the bulk behavior of microstructure-dependent properties, such as the ionic conductivity, is often influenced by the grain boundaries [20]. Then, special care is worth with dopants and co-dopants to avoid adverse effects arising from excessive concentrations. Recently, for example, it was shown that addition of iron oxide to 8 mol% yttria-stabilized zirconia should be limited to 500 ppm to optimize its electrical conductivity [21].

In this work, small amounts of tantalum oxide were added as a co-dopant to zirconia-10 mol% scandia (10ScSZ), aiming to determine its influence on phase transformation, and the minimum amount of co-dopant for stabilization of the cubic structure at room temperature. The effect of the co-dopant on the ionic conductivity of 10ScSZ was also investigated.

## Experimental

### Sample preparation

ZrO<sub>2</sub>-10 mol% scandia, 10ScSZ (99.99%, Daiichi Kigenso Kagaku Kogyo), and tantalum oxide, Ta<sub>2</sub>O<sub>5</sub> (99.9%, Alfa Aesar) were the starting materials. Solid electrolytes of 10ScSZ-*x* mol% Ta<sub>2</sub>O<sub>5</sub> with *x* = 0.25, 0.35, and 0.45 nominal contents were prepared by solid state reactions. The starting materials were dried, weighted in stoichiometric proportions, homogenized in an agate mortar with isopropyl alcohol and dried at 40 °C for 1 h. Cylindrical ( $\phi$  5-mm and 3-mm thickness) specimens of pure 10ScSZ, and mixed powders were prepared by pressing followed by sintering at 1500 °C for 5 h, with 5 °C·min<sup>-1</sup> heating rate and cooling down to room temperature by turning off the furnace (BlueM, Lindberg).

### Characterization

The  $c \rightleftharpoons \beta$ -rhombohedral phase transformation was studied by high-temperature X-ray diffraction, HT-XRD, using a diffractometer (D8 Advance, Bruker-AXS) with  $\theta$ - $\theta$  geometry and equipped with a Braun position sensitive detector and a

heating stage (HTK 1400, Anton Paar). The measurements were carried out in the 47–54°  $2\theta$  range in 0.037° steps, from room temperature, RT ( $\sim 17$  °C) to 600 °C. Differential scanning calorimetry, DSC (404 Pegasus, Netzsch) was also used to investigate the phase transformation from room temperature to 800 °C. The thermal cycle was performed under synthetic air at a flow rate of 20 mL·min<sup>-1</sup> and 10 °C·min<sup>-1</sup> heating rate, with alumina crucible. Spectroscopically pure aluminum was used for DSC calibration. The enthalpy of phase transformation was calculated from the area under the peak recorded during heating. The apparent density of sintered specimens was determined by the immersion method and compared to the theoretical density 5.731 (PDF 89-5482) and 5.740 g·cm<sup>-3</sup> (PDF 89-5483) of the  $\beta$ -rhombohedral and cubic phases, respectively. The apparent porosity was calculated according to ASTM C20-00. The microstructure of sintered specimens was observed by field emission gun scanning electron microscopy, FEG-SEM (Inspect F50, FEI) with secondary electrons on polished and thermally etched surfaces. Room temperature X-ray diffraction, XRD, was carried out for lattice parameter calculation by the Rietveld refinement with GSAS [22]. Experimental patterns were fitted by a pseudo-Voigt function. In this case, the measurements were conducted in a diffractometer (D8 Advance, Bruker-AXS) with  $\theta$ - $2\theta$  geometry, operating at 40 kV and 30 mA with Ni-filtered Cu K $\alpha$  radiation in the 20°  $\leq 2\theta \leq 80$ ° range. The ionic conductivity was determined by impedance spectroscopy, IS, measurements. The pO<sub>2</sub> dependence of the ionic conductivity from 1 to approximately 10<sup>-24</sup> atm at 600, 700, and 800 °C was measured by an impedance/gain phase analyzer (SI 1260, Solartron) in the 1-Hz to 10-MHz frequency range with platinum electrodes. Impedance spectra were analyzed with ZView (Scriber Associates Inc.) software. The temperature dependence of the ionic conductivity at ambient pressure (0.21 atm) was determined by IS with a LF impedance analyzer (4192A, HP) coupled to a 362 model controller in the  $\sim 400$  to 800 °C and 10-Hz to 13-MHz temperature and frequency ranges, respectively. Electrodes of silver (low temperatures, up to  $\sim 550$  °C) and platinum (intermediate temperatures, from  $\sim 550$  to  $\sim 800$  °C) were utilized for electrical measurements. Correction for inductive effects was performed, especially at high temperatures.

## Results and discussion

### Phase transformation

Figure 1 shows HT-XRD patterns of Ta<sub>2</sub>O<sub>5</sub>-doped 10ScSZ specimens in the 47–54° range, where the cubic phase exhibits a single peak at 50.7°, and the  $\beta$ -rhombohedral phase displays two peaks at 50.1° and 51.3°, allowing a

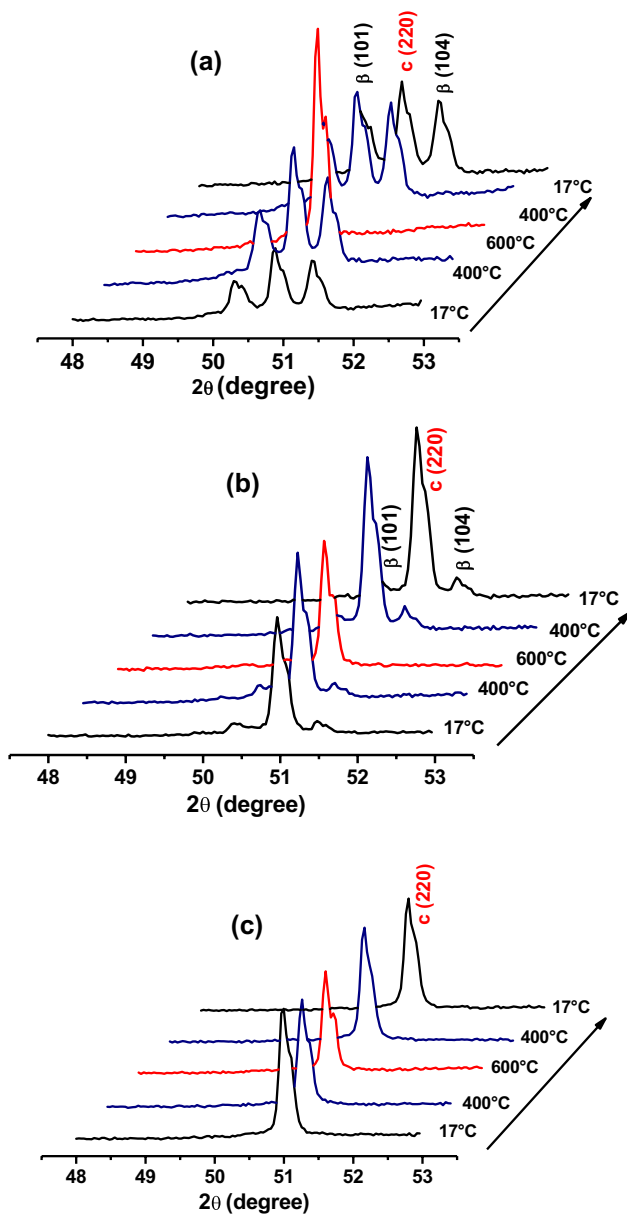


**Fig. 1** HT-XRD patterns of **a** 0.25, **b** 0.35, and **c** 0.45 mol% Ta<sub>2</sub>O<sub>5</sub>-doped 10ScSZ

straightforward identification of both crystalline phases. Miller indexes are shown in parenthesis in these plots, and the direction of the thermal cycle is indicated by arrows. HT-XRD patterns of specimens containing 0.25 (Fig. 1a) and 0.35 mol% Ta<sub>2</sub>O<sub>5</sub> (Fig. 1b), exhibit the (101) and (104) peaks of the  $\beta$ -rhombohedral phase at room temperature and 400 °C during heating and cooling. At 600 °C, these patterns show a single peak characteristic of the cubic structure (220), evidencing the phase transformation in these specimens. The HT-XRD pattern of 0.45 mol% Ta<sub>2</sub>O<sub>5</sub>-doped 10ScSZ (Fig. 1c) reveals a single peak

during the whole thermal cycle corresponding to the cubic phase. These results suggest that the cubic structure of 10ScSZ may be fully stabilized at room temperature with addition of only 0.45 mol% Ta<sub>2</sub>O<sub>5</sub>.

The coefficient of thermal expansion estimated from HT-XRD increases with the co-dopant addition from  $10.3 \cdot 10^{-6}/^{\circ}\text{C}$  to  $15.94 \cdot 10^{-6}/^{\circ}\text{C}$  for pure and 0.45 mol% doped 10ScSZ.

DSC curves of 0.25 and 0.35 mol% Ta<sub>2</sub>O<sub>5</sub>-doped 10ScSZ are shown in Fig. 2a and b, respectively. The reversible cubic  $\rightleftharpoons$   $\beta$ -rhombohedral phase transformation is identified with the endothermic (heating) and exothermic (cooling) peaks recorded during the thermal cycle. The peak temperature of thermal events (indicated in the figure) for both specimens is lower than that of pure 10ScSZ (560 °C during heating [13]). In addition, the maximum amplitude of thermal events decreases with increasing the co-dopant content, indicating a gradual reduction of enthalpy values for phase transformation in Ta<sub>2</sub>O<sub>5</sub>-doped 10ScSZ specimens. It was already shown that the hysteresis of the phase transformation in pure 10ScSZ is about 30 °C [13]. In this case, the specimen with 0.25 mol% Ta<sub>2</sub>O<sub>5</sub> exhibits a hysteresis of 49 °C revealing an increase of the cell volume, which occurs due to incorporation of the co-dopant into the crystal lattice. No thermal events were detected for 10ScSZ containing 0.45 mol% Ta<sub>2</sub>O<sub>5</sub> (Fig. 2c), as a further evidence of the cubic phase stabilization in agreement with HT-XRD results (Fig. 1c).

The calculated values for the enthalpy of phase transformation are 8.78 and 3.20 J·g<sup>-1</sup> for 0.25 and 0.35 mol% Ta<sub>2</sub>O<sub>5</sub>-doped 10ScSZ, respectively. These figures are lower than those obtained for Eu<sub>2</sub>O<sub>3</sub>-doped 10ScSZ [13] supporting that tantalum oxide is more efficient than europium oxide for room temperature cubic phase stabilization of 10ScSZ. In a first approach, this effect seems to be related to the ionic size of co-dopants and the host, such that the lower is the difference between the ionic radii, the lower is the enthalpy for phase stabilization. The mechanism underlying the cubic phase stabilization in co-doped zirconias is still under investigation, with emphasis on acceptor cations. For singly doped zirconias, the cubic phase stabilization is attributed to oxygen vacancies created as charge compensating defects. The distortion produced by these oxygen vacancies would account for the crystal lattice to rearrange itself in a high symmetry structure [23]. In this case, the donor co-dopant with ionic radius (0.074 nm) close to that of Zr<sup>4+</sup> (0.084 nm) is expected to reduce the elastic strain, leading to an increase in the degree of the short-range disorder in the anion sublattice. Similar finding was observed by neutron diffraction, molecular dynamic, and reverse Monte Carlo simulation for niobium-doped zirconia [24].

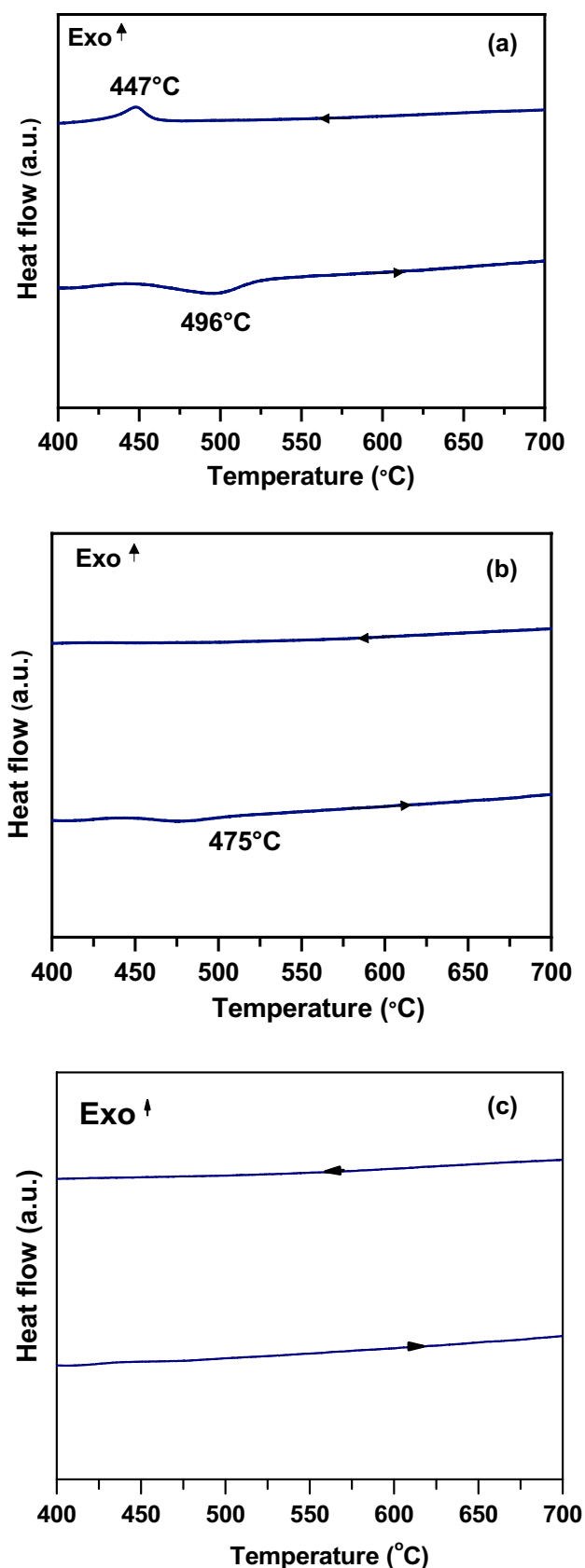


**Fig. 2** DSC curves of 10ScSZ containing **a** 0.25, **b** 0.35, and **c** 0.45 mol% Ta<sub>2</sub>O<sub>5</sub>

**Table 1** Density and porosity values of sintered pure and co-doped 10ScSZ

Ta <sub>2</sub> O <sub>5</sub> (mol%)	Relative density (± 0.5%)	Apparent porosity (± 0.3%)	Phase composition
-	97.5	0.6	β
0.25	95.9	1.2	β + c
0.35	95.6	1.2	β + c
0.45	97.9	1.4	c

### Microstructure

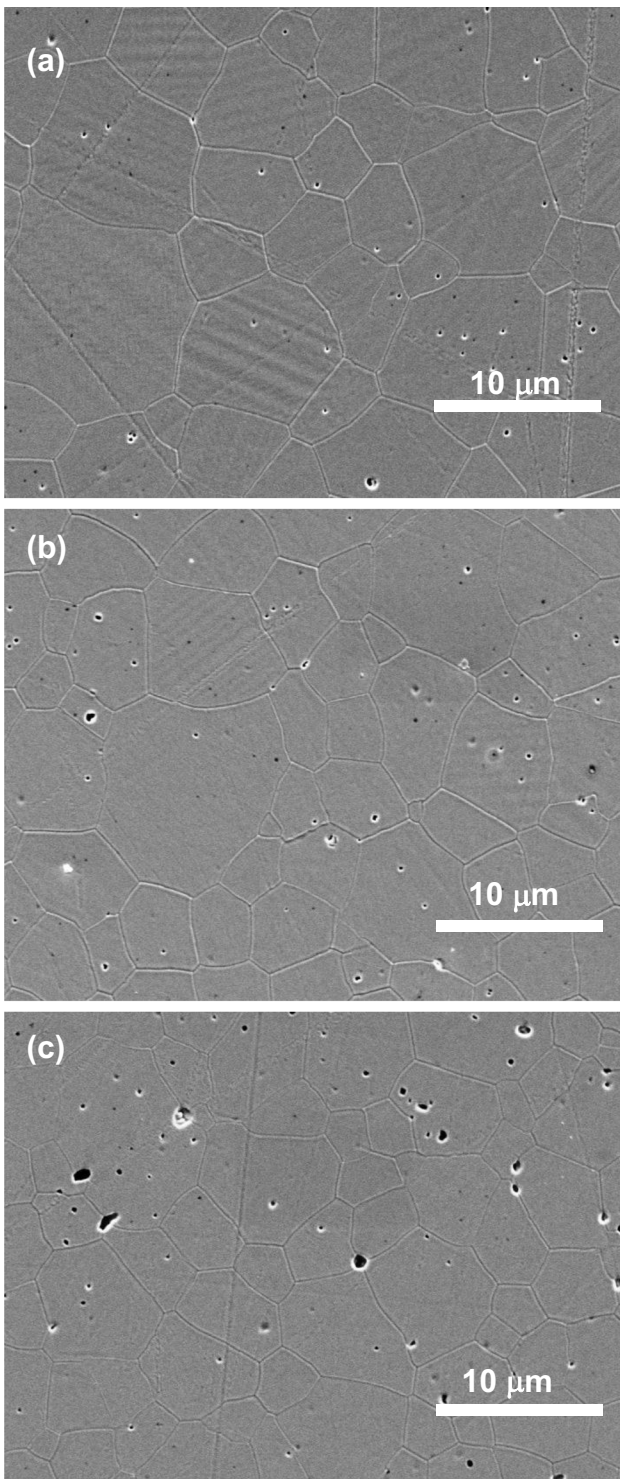
Table 1 lists density and porosity data obtained for sintered specimens. Relatively high densities ( $\geq 95\%$  of the theoretical value) and low porosity ( $< 2\%$ ) were obtained for all pure and co-doped specimens.

Figure 3 shows typical FEG-SEM micrographs of Ta<sub>2</sub>O<sub>5</sub>-doped 10ScSZ. The main microstructure features are large and polygonal grains with average size in the 5–7- $\mu\text{m}$  range. Pores are found along the grain boundaries and inside the grains. No undesirable features like abnormal grain growth, cracks, or dopant segregation were found. Several grains of the specimen containing 0.25 mol% Ta<sub>2</sub>O<sub>5</sub> (Fig. 3a) exhibit a herringbone structure characteristic of the  $c \rightleftharpoons \beta$ -rhombohedral phase transformation. The same occurs for 0.35 mol% (Fig. 3b) specimen, though to a less extent. This microstructure feature is not observed in the micrograph of 0.45 mol% Ta<sub>2</sub>O<sub>5</sub>-doped 10ScSZ (Fig. 3c) highlighting the absence of phase transformation, in this case.

Room temperature XRD patterns of pure and Ta<sub>2</sub>O<sub>5</sub>-doped 10ScSZ in the whole  $2\theta$  range are depicted in Fig. 4a, and the phase composition is summarized in Table 1. The XRD pattern of pure 10ScSZ corresponds to that of  $\beta$ -rhombohedral phase (PDF 89-5482), whereas that of specimen containing 0.45 mol% tantalum oxide agrees with the XRD profile of the cubic phase (PDF 89-5483). Other specimens show diffraction peak characteristics of a mixture of cubic and  $\beta$ -rhombohedral phases. These results are in general agreement with those of HT-XRD (Fig. 1) and DSC (Fig. 2).

The room temperature XRD pattern and the Rietveld refinement of 0.45 mol% Ta<sub>2</sub>O<sub>5</sub>-doped 10ScSZ specimen are shown in Fig. 4b. Small marks in the bottom denote the Bragg position of the cubic phase, and the difference between the experimental and the refined profiles is the line below the diffractograms. The experimental and refined profiles agree with each other within experimental uncertainties, with  $\chi^2$  equal to 3.5. The calculated lattice parameter, 0.5086 nm, is slightly lower than that of pure 10ScSZ ( $\sim 0.5092$  nm [12]), due to incorporation of tantalum into the zirconia lattice.





**Fig. 3** FEG-SEM micrographs of **a** 0.25, **b** 0.35, and **c** 0.45 mol% Ta<sub>2</sub>O<sub>5</sub>-doped 10ScSZ

**Ionic conductivity**

Figure 5a shows  $[-Z''(\omega) \times Z'(\omega)]$  plots of co-doped 10ScSZ specimens, where  $-Z''(\omega)$  stands for the imaginary and  $Z'(\omega)$

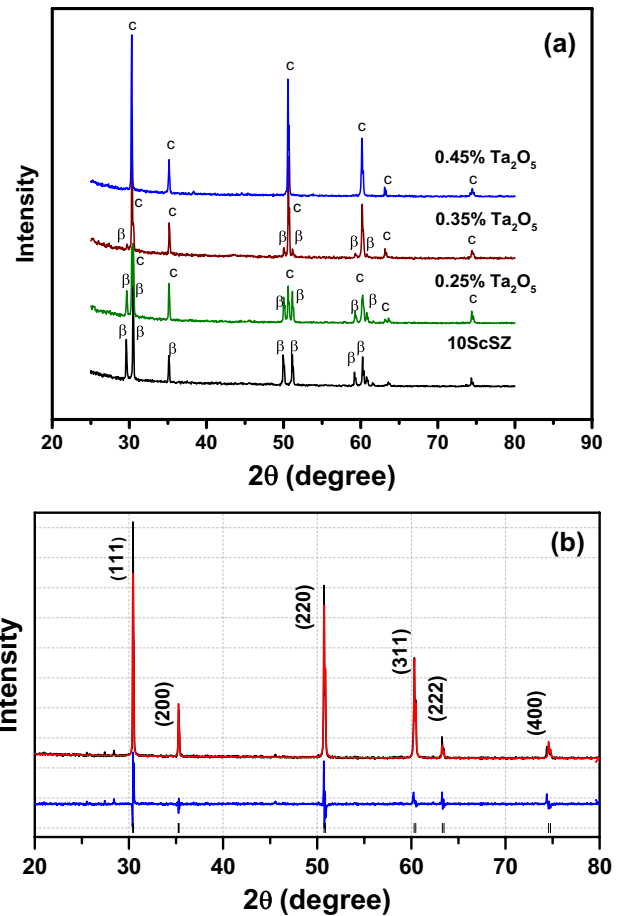


**Fig. 4 a** Room temperature XRD patterns of pure 10ScSZ and co-doped specimens, and **b** Rietveld refinement of the 0.45 mol% Ta<sub>2</sub>O<sub>5</sub>-doped 10ScSZ

for the real components of the impedance. The temperature of measurement was 406 °C, and the impedance components were normalized for specimen dimensions. Numbers in these plots are the relaxation frequencies (Hz). Similar shape is exhibited by all impedance plots comprising a large arc at high frequencies, attributed to the bulk or grain resistivity, a low intensity arc in the intermediate frequency range, assigned to the grain boundary resistivity, and a low frequency spike, due to reactions at the electrolyte/electrode interface. The resistivity of each constituent of the electrolyte (bulk and grain boundary) was determined in the real intercept at the low frequency side of every component, and the relaxation frequency,  $f$ , obtained at the maximum amplitude of arcs is characteristic of the corresponding phenomenon [25]. Some degree of overlapping is seen in these plots between the bulk and the grain boundary arcs.

Arrhenius plots of total electrolyte conductivity (bulk and grain boundary) in the low temperature ( $\leq 550$  °C) range are shown in Fig. 5b. Experimental data are represented by symbols and lines are the fitting. The sintered specimens display

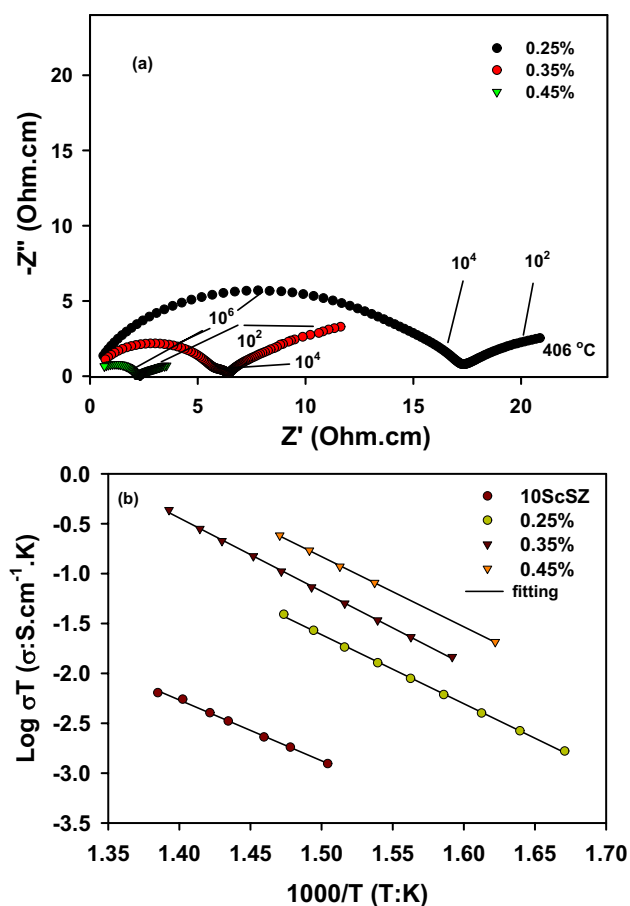


**Fig. 5** **a** Impedance spectroscopy diagrams of  $\text{Ta}_2\text{O}_5$ -doped 10ScSZ, **b** Arrhenius plots of total (bulk and grain boundary) conductivity of pure 10ScSZ and co-doped specimens in the low temperature range. Ag electrodes

a single straight line with an average activation energy value of  $1.32 \pm 0.08$  eV, which agrees with previous reports on other co-doped systems [7, 11, 12]. In the restricted temperature range of measurements, the conductivity of pure 10ScSZ and that of co-doped specimens greatly differs. Pure 10ScSZ exhibits very low conductivity values consistent with that of the  $\beta$ -rhombohedral phase. In contrast, co-doped specimens exhibit higher values of ionic conductivity, achieving a maximum for 0.45 mol%  $\text{Ta}_2\text{O}_5$ -doped 10ScSZ specimen. At 400 °C, for example, the total electrolyte conductivity amounts 0.00247 (10ScSZ), 0.0493 (0.25 mol%), 0.127 (0.35 mol%) and 0.464  $\text{mS}\cdot\text{cm}^{-1}$  (0.45 mol%).

The evolution of the relaxation frequency of the bulk,  $f_b$ , is plotted in Fig. 6 for pure and co-doped 10ScSZ specimens in the same temperature range (up to  $\sim 550$  °C). Formerly, this type of plot was used to highlight the closeness among the different components of total impedance [25]. In this case, this plot is utilized to evidence the progress of the relaxation frequency with the process of cubic phase stabilization. Different specimens with 0.45 mol%  $\text{Ta}_2\text{O}_5$

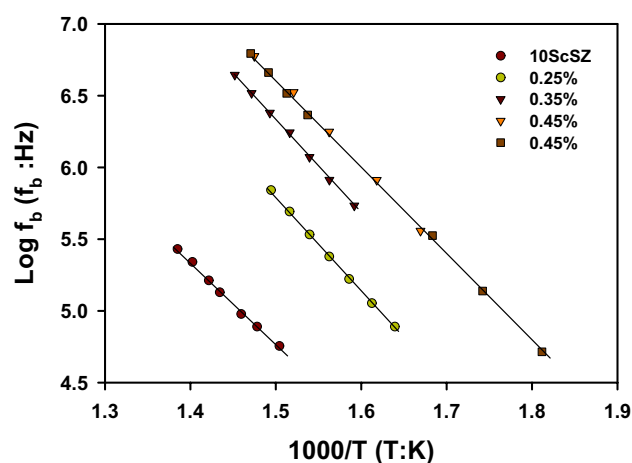


**Fig. 6** Relaxation frequency plots of the bulk of sintered specimens

(represented in this figure with dissimilar symbols) were measured to ensure reproducibility. At any fixed temperature, it may be noted the large increase of  $f_b$  with increasing co-dopant content. That increase is very large from pure 10ScSZ to 0.25 mol%  $\text{Ta}_2\text{O}_5$ -doped 10ScSZ and slows down with additional increase of the co-dopant content. This kind of evolution of  $f_b$  suggests saturation when the cubic phase is fully stabilized, and a straight relationship between this parameter and the concentration of oxygen vacancies available for conduction. These findings are further evidences of changes promoted by incorporation of tantalum oxide in the bulk of 10ScSZ.

The  $\text{pO}_2$  dependence of the total electrical conductivity at 600, 700, and 800 °C of the 0.45 mol%  $\text{Ta}_2\text{O}_5$ -doped 10ScSZ specimen is shown in Fig. 7. Typical ionic behavior with

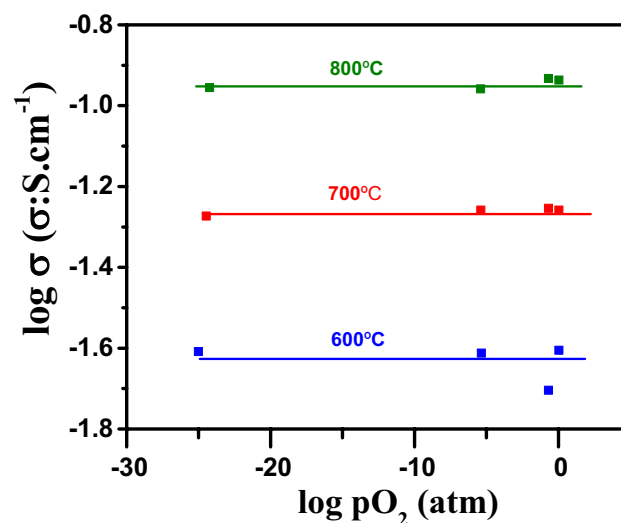


**Fig. 7** Total electrical conductivity versus  $\text{pO}_2$  of 0.45 mol%  $\text{Ta}_2\text{O}_5$  co-doped 10ScSZ specimens. Pt electrodes

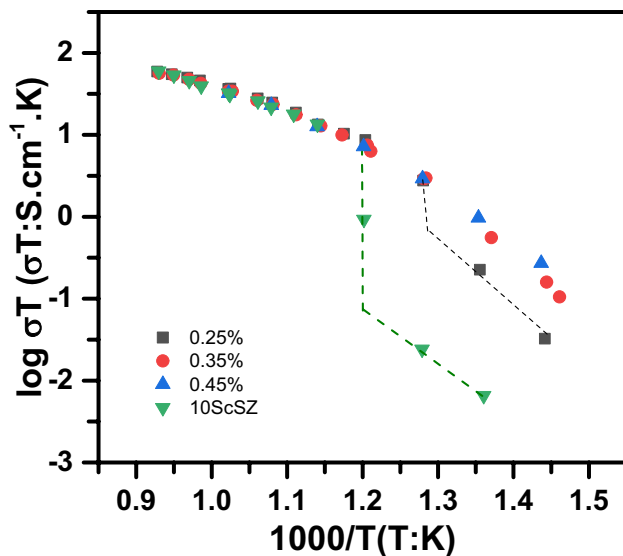


**Fig. 8** Arrhenius plots of the bulk conductivity in the intermediate temperature range. Pt electrodes. Lines are guide to eyes

wide electrolytic domain is seen in these plots, evidencing no change of valence of the co-dopant even in severe reducing environments, such as that at the anode side of solid oxide cells.

It is generally recognized that introduction of a donor dopant or co-dopant into the zirconia lattice may lead to undesirable effects, such as reduction of the concentration of oxygen vacancies available for conduction and/or increase of the electronic conductivity with simultaneous decrease of the activation energy. In this case, those undesirable effects may be occurring, but simultaneously with the advantageous effect of cubic phase stabilization. In addition, considering the small amount of the co-dopant, those undesirable effects should be negligible. Other issues to be taken into account are cation coordination and interstitial oxygen occupancy in co-doped ceramics, along with reduction of defect association. The latter was found in co-doped cerium oxide by high-temperature oxide melt solution calorimetry, accounting for the high ionic conductivity of the doubly doped system [26]. All these features are able to change the ionic conductivity of solid electrolytes, and additional studies on both experimental and modeling are worth to clarify their exact role in co-doped zirconia-scandia.

Figure 8 depicts Arrhenius plots of the bulk conductivity in the intermediate temperature range. The bulk conductivity of pure and co-doped 10ScSZ specimens exhibits interesting features. For temperatures up to  $\sim 600$  °C, pure, 0.25, and 0.35 mol% Ta<sub>2</sub>O<sub>5</sub>-doped 10ScSZ display a jump in the conductivity, whose magnitude and temperature depend upon the co-dopant content. That jump is barely seen for the 0.35 mol% Ta<sub>2</sub>O<sub>5</sub>-doped 10ScSZ specimen, whereas it amounts more than two orders of magnitude for pure 10ScSZ. Then,

the lower is the fraction of co-dopant, the higher is the temperature and the magnitude of the jump in conductivity. For temperatures above approximately 600 °C, the ionic conductivity of different specimens converges, and becomes similar under experimental uncertainties. This is probably due to the very low amounts of the co-dopant in 10ScSZ, and because at such temperature and above, the ionic conductivity corresponds to that of the cubic phase for all specimens.

The higher total ionic conductivity reported for several trivalent co-dopants (1 mol%) in 10ScSZ was found for Yb<sub>2</sub>O<sub>3</sub> (14 mS·cm<sup>-1</sup> at 600 °C [12]). In this case, neglecting the grain boundary contribution that is marginal for Ta<sub>2</sub>O<sub>5</sub>-doped 10ScSZ (see Fig. 5a), the grain conductivity determined from Fig. 8 at 600 °C amounting 14.3 mS·cm<sup>-1</sup>, is similar to that of ytterbium co-doped zirconia-scandia.

The ionic conductivity and the activation energy for the bulk may be considered similar to the total conductivity, in the 700–800 °C range, since the blocking of charge carriers at grain boundaries vanishes [11, 25]. Activation energy values determined in the 700–800 °C are  $0.64 \pm 0.05$  eV corresponding to the oxygen vacancy migration energy, in agreement with previous reports [10, 11].

The overall results evidence the positive effects of tantalum oxide for stabilization of the cubic phase at room temperature and to increase the ionic conductivity of scandia-doped zirconia at low temperatures. Moreover, co-doped specimens with 0.45 mol% reveal high ionic conductivity even in reducing pO<sub>2</sub>, without reduction of the conductivity at intermediate temperatures. These findings turn this new co-doped system a candidate for application as solid electrolyte in solid oxide cells operating at intermediate temperatures.

## Conclusions

Reduction of the enthalpy associated to the cubic  $\rightleftharpoons$   $\beta$ -rhombohedral phase transformation of 10ScSZ was obtained with increasing amounts of tantalum oxide. Full stabilization of the cubic phase at room temperature was achieved with only 0.45 mol% Ta<sub>2</sub>O<sub>5</sub>. The co-dopant was also responsible for increasing the ionic conductivity of 10ScSZ in the low temperature range. The 0.45 mol% Ta<sub>2</sub>O<sub>5</sub>-doped 10ScSZ showed a high resistance to reduction up to 800 °C in a wide range of oxygen partial pressures, ensuring the ionic character of the conductivity.

**Acknowledgements** The authors acknowledge DKKK for providing the 10ScSZ sample.

**Funding** This work was financially supported by FAPESP (2013/07296-2), CNPq (305889/2018-4), CAPES (88887.371190/2019-00), and CNEN.

## Declarations

**Conflict of interest** The authors declare no competing interests.

## References

- Garvie RC, Hannink RH, Pascoe RT (1975) Ceramic steel? *Nature* 258:703–704. <https://doi.org/10.1038/258703a0>
- Subbarao EC (1981) Zirconia-an overview. In: Heuer AH, Hobbs LW (eds) *Advances in Ceramics v. 3 - Science and Technology of Zirconia I*. The American Ceramic Society, Columbus, Ohio, pp 1–24 ISBN: 0-916094-42-1
- Dell RM, Hooper A (1978) Oxygen ion conductors. In: Hagemuller P, Van Gool W (eds) *Solid electrolytes, general principles, characterization, materials, applications*. Academic Press, New York, pp 291–312 ISBN: 0-12-313360-2
- Ruh R, Garrett HJ, Domagala RF, Patel VA (1977) The system zirconia-scandia. *J Am Ceram Soc* 60:399–403. <https://doi.org/10.1111/j.1151-2916.1977.tb15521.x>
- Abdala PM, Fantini MCA, Craievich AF, Lamas DG (2010) Crystallite size-dependent phases in nanocrystalline  $ZrO_2$ - $Sc_2O_3$ . *Phys Chem Chem Phys* 12:2822–2829. <https://doi.org/10.1039/b922541b>
- Grosso RL, Muccillo ENS, Castro RHR (2017) Enthalpies of formation in the scandia-zirconia system. *J Am Ceram Soc* 100:4270–4275. <https://doi.org/10.1111/jace14945>
- Badwal SPS, Ciacchi FT, Milosevic D (2000) Scandia-zirconia electrolytes for intermediate temperature solid oxide fuel cell operation. *Solid State Ionics* 136-137:91–99. [https://doi.org/10.1016/S0167-2738\(00\)00356-8](https://doi.org/10.1016/S0167-2738(00)00356-8)
- Fujimori H, Yashima M, Kakihana M, Yoshimura M (2002)  $\beta$ -cubic phase transition of scandia-doped zirconia solid solution: calorimetry, X-ray diffraction, and Raman scattering. *J Appl Phys* 91:6493–6498. <https://doi.org/10.1063/1.1471576>
- Spiridonov FM, Popova LN, Popil'skii RY (1970) On the phase relations and the electrical conductivity in the system  $ZrO_2$ - $Sc_2O_3$ . *J Solid State Chem* 2:430–438. [https://doi.org/10.1016/0022-4596\(70\)90102-7](https://doi.org/10.1016/0022-4596(70)90102-7)
- Arachi Y, Asai T, Yamamoto O, Takeda Y, Imanishi N, Kawate K, Tamakoshi C (2001) Electrical conductivity of  $ZrO_2$ - $Sc_2O_3$  doped with  $Hf_2O_3$ ,  $CeO_2$  and  $Ga_2O_3$ . *J Electrochem Soc* 148:A520–A523. <https://doi.org/10.1149/1.1366622>
- Politova TI, Irvine JTS (2004) Investigation of scandia-yttria-zirconia system as an electrolyte material for intermediate temperature fuel cells-influence of yttria content in system  $(Y_2O_3)_x(Sc_2O_3)_{0.11-x}(ZrO_2)_{0.89}$ . *Solid State Ionics* 168:153–165. <https://doi.org/10.1016/j.ssi.2004.02.007>
- Omar S, Najib WB, Chen W, Bonanos N (2012) Electrical conductivity of 10 mol%  $Sc_2O_3$ -1 mol%  $M_2O_3$ - $ZrO_2$  ceramics. *J Am Ceram Soc* 95:1965–1972. <https://doi.org/10.1111/j.1551-2916.2012.05126.x>
- Souza JP, Grosso RL, Muccillo R, Muccillo ENS (2018) Phase composition and ionic conductivity of zirconia stabilized with scandia and europia. *Mater Lett* 229:53–56. <https://doi.org/10.1016/j.matlet.2018.06.091>
- Bai B, Sammes NM, Smirnova AL (2008) Physical and electrochemical characterization of  $Bi_2O_3$ -doped scandia stabilized zirconia. *J. Power Sources* 176:76–81. <https://doi.org/10.1016/j.jpowsour.2007.10.074>
- Wang Z, Cheng M, Bi Z, Dong Y, Zhan H, Zhang J, Feng Z, Li C (2005) Structure and impedance of  $ZrO_2$  doped with  $Sc_2O_3$  and  $CeO_2$ . *Mater Lett* 59:2579–2582. <https://doi.org/10.1016/j.matlet.2004.07.065>
- Grosso RL, Muccillo R, Muccillo ENS (2014) Stabilization of the cubic phase in zirconia-scandia by niobium oxide addition. *Mater Lett* 134:27–29. <https://doi.org/10.1016/j.matlet.2014.07.039>
- Shukla V, Singh S, Subramaniam A, Omar S (2020) Long-term conductivity stability of metastable tetragonal phases in  $1Yb_2O_3$ - $xSc_2O_3$ - $(99-x)ZrO_2$  ( $x=7, 8$  mol%). *J Phys Chem C* 124:23490–23500. <https://doi.org/10.1021/acs.jpcc.0c05298>
- Agarkov DA, Borik MA, Bredikhin SI, Burmistrov IN, Eliseeva GM, Kulebyakin AV, Kuritsyna IE, Lomonova EE, Milovich FO, Myzina VA, Tabachkova NY (2020) Phase compositions, structures and properties of scandia-stabilized zirconia solid solution crystals co-doped with yttria or ytterbia and grown by directional melt crystallization. *Solid State Ionics* 346:115218. <https://doi.org/10.1016/j.ssi.2019.115218>
- Zhigachev AO, Rodaev VV, Zhigacheva DV, Lyskov NV, Shchukina MA (2021) Doping of scandia-stabilized zirconia electrolytes for intermediate-temperature solid oxide fuel cell: a review. *Ceram Int* 47:32490–32504. <https://doi.org/10.1016/j.ceramint.2021.08.285>
- Rohrer GS, Affatigato M, Backhaus M, Bordia RK, Chan HM, Curtarolo S, Demkov A, Eckstein JN, Faber KT, Garay JF, Gogotsi Y, Huang L, Jones LE, Kalinin SV, Lad RJ, Levi CG, Levy J, Maria J-P, Mattos L Jr et al (2012) Challenges in ceramic science: a report from the workshop on emerging research areas in ceramic science. *J Am Ceram Soc* 95:3699–3713. <https://doi.org/10.1111/jace12033>
- Jeon OK, Park MG, Song RH, Ryu KH, Na CW, Shul YG, Lee JG (2022) Effects of  $Fe_2O_3$  doping on structural and electrical properties of 8 mol% yttria-stabilized zirconia electrolyte for solid oxide fuel cells. *J Mater Sci Mater Electron* 33:3208–3214. <https://doi.org/10.1007/s10854-021-07522-w>
- Larson AC, von Deele RB (1994) General structure analysis system (GSAS). Los Alamos Laboratory Report, LAUR, pp 86–748
- Raza M, Cornil D, Cornil J, Lucas S, Snyders R, Konstantinides S (2016) Oxygen vacancy stabilized zirconia (OVSZ); a joint experimental and theoretical study. *Scr Mater* 124:26–29. <https://doi.org/10.1016/j.scriptamat.2016.06.025>
- Norberg ST, Ahmed I, Hull S, Marrochelli D, Madden PA (2009) Local structure and ionic conductivity in the  $Zr_2Y_2O_7$ - $Y_3NbO_7$  system. *J Phys Condens Matter* 21:215401. <https://doi.org/10.1088/0953-8984/21/21/215401>
- Kleitz M, Bernard H, Fernandez E, Schouler E (1981) Impedance spectroscopy and electrical resistance measurements on stabilized zirconia. In: Heuer AH, Hobbs LW (eds) *Advances in ceramics, v. 3 - Science and Technology of Zirconia I*. The American Ceramic Society, Columbus OH, pp 310–336 ISBN: 0-916094-42-1
- Buyukkilic S, Shvareva T, Navrotsky A (2012) Enthalpies of formation and insights into defect association in ceria singly and doubly doped with neodymia and samaria. *Solid State Ionics* 227:17–22. <https://doi.org/10.1016/j.ssi.2012.08.017>

**Publisher's note** Springer Nature remains neutral with regard to jurisdictional claims in published maps and institutional affiliations.